ChemComm

COMMUNICATION

View Article Online
View Journal

Cite this: DOI: 10.1039/d6cc01405d

Received 10th March 2026,
Accepted 15th April 2026

DOI: 10.1039/d6cc01405d

rsc.li/chemcomm

Effect of alkyl spacer length of thienyl-substituted carbazole-type self-assembled monolayers on the performance of inverted perovskite solar cells

Nobuko Onozawa-Komatsuzaki, *[a] Atsushi Kogo, [a] Takuma Chigira,[ab] Hiroyuki Yaguchi, [b] Masayuki Chikamatsu, [a] Takashi Funaki *[a] and Takurou N. Murakami *[a]

We synthesized thienyl-substituted carbazole-type self-assembled monolayers with different alkyl spacer lengths and evaluated their performance when used as hole transport layers in inverted perovskite solar cells. Among them, T-4PACz with butylene spacers showed the highest power conversion efficiency and thermal stability due to improved solubility and film formation.

Organic–inorganic hybrid perovskite solar cells (PSCs) are among the most remarkable advancements in emerging photovoltaic technologies, comparable to silicon solar cells, because of their outstanding power conversion efficiency (PCE).[1–3] However, most PSCs have achieved their highest efficiencies using an n–i–p structure based on a mesoporous scaffold (*i.e.*, a SnO_2 or TiO_2 layer).[4,5] By contrast, the PCE for i-PSCs with an inverted structure (p–i–n) has lagged behind. However, in recent years, p–i–n-structured i-PSCs have been reported to demonstrate PCEs equivalent to those of n–i–p PSCs.[6–9] In addition, i-PSCs without TiO_2 layers have recently been attracting attention because they are suitable for roll-to-roll mass production on flexible plastic substrates as a result of their easy adaptation to low-temperature solution processes, which is expected to lead to reduced fabrication costs.[10–12] The key components of the architecture of conventional i-PSCs are an n-type semiconductor (electron-collecting material), a hybrid organic–inorganic perovskite sensitizer, a p-type semiconductor (hole transport layer, HTL), and a metal electrode. In addition to film and interfacial engineering of the perovskite layer, the development of HTLs is extremely important for improving the device performance of i-PSCs because the HTL plays a crucial role in achieving high performance through efficient hole extraction from the perovskite, hole transport to the indium tin oxide (ITO) side, and a resultant reduction in charge recombination.[13,14]

Recently, self-assembled monolayers (SAMs) have been used as HTLs for i-PSCs because they have the advantages of excellent conformal coating ability on irregular surfaces, low optical loss, low material consumption, and easily adjusted energy levels.[15] Therefore, the use of SAMs as HTLs has contributed greatly to improving the efficiency of i-PSCs.[16] In particular, SAMs with a carbazole core and phosphonic acid anchor are widely used as HTLs in i-PSCs and contribute to efficiency improvements not only in single-junction devices but also in perovskite-based tandem solar cells.[17,18] These improvements stem from the phosphonic acid anchor forming densely packed molecules on ITO by creating strong bidentate/tri-dentate bonds.[19] For example, carbazole-type SAMs such as [2-(9*H*-carbazol-9-yl)ethyl]phosphonic acid (**2PACz**), [4-(9*H*-carbazol-9-yl)ethyl]phosphonic acid (**4PACz**), and [2-(3,6-dimethoxy-9*H*-carbazol-9-yl)ethyl]phosphonic acid (**MeO-2PACz**) have led to the realization of high-efficiency i-PSCs.[20,21] In addition, they exhibit a fast hole transfer rate, a high hole selectivity, and a low density of interface traps.[16,22]

In the present study, we synthesized four carbazole-type SAMs (**T-PACz**, **T-2PACz**, **T-3PACz**, and **T-4PACz**) with different alkyl spacer lengths. All of them have a thienyl-substituted carbazole unit, and such thienyl groups are known to passivate interface defects in perovskite absorbers.[23,24] In the case of n–i–p PSCs, Wen *et al.* demonstrated that the π-conjugated structure of a thiophene ring could easily coordinate with surface Pb^{2+} and that the delocalized π-electrons occupied the vacuum orbitals of Pb^{2+}, which contributed to efficient hole extraction.[23] However, in the case of i-PSCs, Wan *et al.* reported that SAMs with thienyl groups lead to electrostatic interactions between the S atom in the thiophene and under-coordinated Pb^{2+} and S atoms in the perovskite layer.[25] Very recently, Ai *et al.* synthesized a new carbazole-type SAM with thienyl groups and demonstrated its application in a high-efficiency PSC.[26] Although various carbazole-type SAMs have been reported thus far,[16] the literature contains few reports comparing their performance on the basis of differences in alkyl chain length.[22] Therefore, in the present study, we investigated how the length of the alkyl chain in four different SAMs affects the

[a] *National Institute of Advanced Industrial Science and Technology (AIST), Central 5, 1-1-1 Higashi Tsukuba, Ibaraki 305-8565, Japan. E-mail: n-onozawa@aist.go.jp*
[b] *Graduate School of Science and Engineering, Saitama University, 255 Shimo-Okubo, Sakura-ku, Saitama 338-8570, Japan*

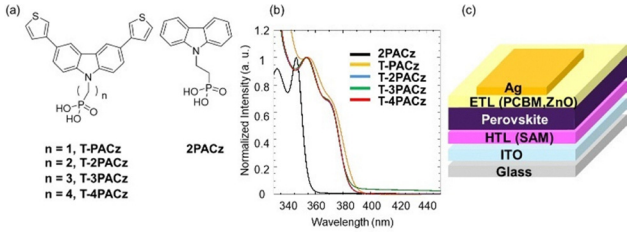

Fig. 1 (a) Molecular structure of SAMs investigated in present study, along with that of **2PACz** used as reference, (b) UV-vis spectra of SAMs prepared as solutions in DMF and (c) structure of i-PSCs used in present study.

performance of i-PSCs fabricated using these SAMs as HTLs. We expect this structural approach to be advantageous in the context of SAM-based interfacial materials.

The molecular structures of the four synthesized carbazole-based SAMs (**T-PACz**, **T-2PACz**, **T-3PACz**, and **T-4PACz**) and **2PACz** as a reference compound are shown in Fig. 1(a); details of their synthesis are provided in Scheme S1 and their ^{1}H nuclear magnetic resonance (NMR) spectra are shown in Fig. S1–S4. The four SAMs incorporate a thienyl group into the carbazole group. Passivating the perovskite layer is well known to be crucial for improving device efficiency.[24] In addition, molecules used to modify the surface of perovskite layers must exhibit excellent electrical conductivity.[27] Among such molecules, thiophene derivatives feature an electron-rich π-conjugated structure consisting of two lone-pair electrons from the S atom and four 2p orbital electrons from C atoms.[28] We therefore introduced a thiophene ring into the carbazole group of the SAM molecules. To gain insight into the interaction between the thiophene group and the perovskite, we carried out NMR analyses using PbI_2, which was adopted to mimic uncoordinated Pb^{2+} ions in a perovskite film. As shown in Fig. S5, slight down-field shifts of the proton peaks were observed in the ^{1}H NMR spectrum of a solution of **T-2PACz** after PbI_2 was added. Comparing the spectrum of **T-2PACz** with that of **T-2PACz** in the presence of PbI_2 reveals that the height and shape of the peaks around 7.70 ppm, where two thiophene peaks are overlapped, differ. These differences mean that the peak shifts differ between these protons. These shifts and their variation suggest that the S atom in the thiophene group interacts with Pb^{2+}, and this interaction might affect the formation of the perovskite film.

The optical and electrochemical properties of the SAM molecules are summarized in Table S1. The ultraviolet–visible (UV-vis) absorption spectra of the SAM molecules in *N*,*N*-dimethylformamide (DMF) are presented in Fig. 1(b). The energy levels for the SAMs are shown in Fig. S6. None of the SAMs exhibits absorption at wavelengths longer than 400 nm, indicating their transparency to visible radiation. Compared with the absorption maximum for **2PACz**, those for SAMs are redshifted, and this is attributed to the extension of the π-conjugated structure on the aromatic rings.[29] However, there is no significant dependence of the absorption spectra on the alkyl chain length. From the absorption onset in the spectra, the optical bandgap (E_g) for all of the SAMs is calculated to be in the range 3.20–3.23 eV. The introduction of thienyl groups causes a decrease in E_g, as evidenced by the redshift of the absorption peak assigned to π–π* transitions. The highest occupied molecular orbital (HOMO) energy levels for all of the SAMs were obtained by differential pulse voltammetry (DPV) after they were dissolved in DMF and tetrabutylammonium perchlorate ($TBAClO_4$) (0.1 M). The lowest unoccupied molecular orbital (LUMO) energy levels were calculated from the HOMO and E_g values. The HOMO energy levels for the thienyl-substituted carbazole-type SAMs were estimated to range from −5.34 to −5.37 eV, which are higher than that for **2PACz** because of their electron-donating thiophene ring. By contrast, the LUMO energy levels for the thienyl-substituted carbazole-based SAMs are approximately the same as that for **2PACz**. Thus, these results show that the SAMs have suitable energy levels for hole extraction from perovskites.

The thienyl-substituted carbazole-type SAMs were used as HTLs in i-PSCs with a device configuration of ITO/SAM/perovskite/[6,6]-phenyl-C_{61}-butyric acid methyl ester (PCBM)/ZnO/Ag to evaluate their effectiveness [Fig. 1(c)]. $Cs_{0.05}(FA_{0.83}MA_{0.17})_{0.95}Pb(I_{0.83}Br_{0.17})_3$ (MA = methylammonium (CH_3NH_3); FA = formamidinium ($CH(NH_2)_2$)) perovskites were formed on SAMs as HTLs using our previously reported method.[30] The photovoltaic data obtained from the PSCs are summarized in Table S2. Current density–voltage (*J*–*V*) curves for the best-performing PSCs with various SAMs are shown in Fig. 2(a) and Fig. S7 and S8. The reference device based on **2PACz** shows a PCE of 16.0% with an open-circuit voltage (V_{oc}) of 1.10 V, a short-circuit current density (J_{sc}) of 20.9 mA cm^{-2}, and a fill factor (FF) of 0.70 (forward scan) under 1-sun illumination (AM 1.5G and 100 mW cm^{-2}). The PCEs for the PSCs fabricated using **T-PACz**, **T-2PACz**, **T-3PACz**, and **T-4PACz** were 15.8%, 15.9%, 16.2%, are 16.9%, respectively. Thus, the PSC based on **T-4PACz** afforded the highest PCE in the present study. External quantum efficiency (EQE) spectra are shown in Fig. S9. The spectra for all of the PSCs based on the SAMs investigated in the present study are similar to each other. For the PSCs based on the thienyl-substituted carbazole-type SAMs, both V_{oc} and J_{sc} show similar values, likely because

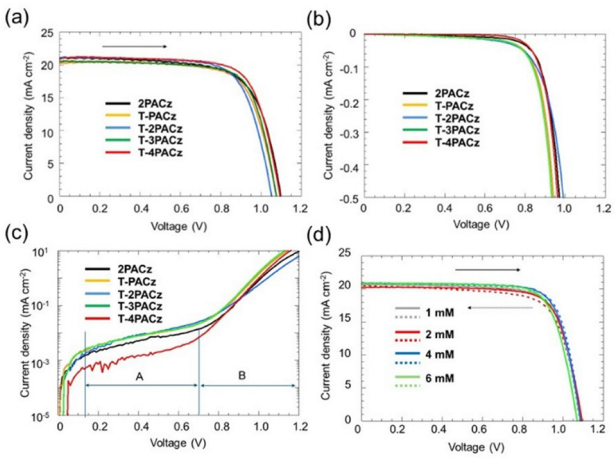

Fig. 2 (a) *J*–*V* curves for PSCs based on SAMs, as measured using forward scans. (b) Dark *J*–*V* curves for PSCs based on SAMs (backward scans). (c) Dark *J*–*V* curves for PSCs based on SAMs (forward scans). (d) *J*–*V* curves for PSCs based on **T-4PACz**.

the HOMO levels for the SAMs are similar. However, the PSC based on **T-4PACz** exhibits the highest FF value among the investigated devices. **T-4PACz** has butylene spacers, which are the longest alkyl spacers used in the present study; thus, among the investigated SAMs, it exhibits the highest solubility in organic solvents. Consequently, **T-4PACz** is considered to exhibit the best film-forming properties among the thienyl-substituted carbazole-type SAMs. However, top-view scanning electron microscopy (SEM) observations of the perovskite substrates based on the various SAMs indicate no differences in surface morphology (Fig. S10). The dark *J*–*V* behavior was analyzed to compare the diode properties of the PSCs under dark conditions [Fig. 2(b) and (c)]. The PSCs based on **T-4PACz** exhibit a higher onset voltage (0.7 V) than those based on the other SAMs (0.5 V). **T-4PACz** has butylene spacers, imparting it with greater solubility in organic solvents compared with other SAMs. It therefore exhibits excellent film-forming properties and can uniformly coat the surface of ITO, leading to reduced dark-current leakage and enhanced carrier-current rectification in PSCs than in the case of SAMs having shorter alkyl spacers.[31] We also compared the recombination current [region A in Fig. 2(c)] and diffusion current [region B in Fig. 2(c)] in the dark *J*–*V* experiments to examine the ease of current flow. The PSC based on **T-4PACz** exhibits a slightly higher diffusion current (region B) and a lower recombination current (region A) than the PSCs based on other SAMs. These results indicate that the PSC based on **T-4PACz** has a low trap density. For the PSC based on **T-4PACz**, the excellent film-forming properties of **T-4PACz** as a result of its long alkyl spacers suppresses charge-carrier recombination.

We carried out steady-state photoluminescence (PL) and time-resolved photoluminescence (TRPL) measurements to determine the hole extraction capability of the HTLs. As shown in Fig. S11(a), the steady-state PL spectra of the ITO/thienyl-substituted carbazole-type SAM/perovskite devices are lower in intensity than those of the ITO/**2PACz**/perovskite device, which suggests stronger hole extraction capabilities. This is speculatively attributed to the passivation effect of the thienyl groups,[25] and is consistent with the faster PL decay observed during TRPL measurements of carbazole-type SAM-based devices [Fig. S11(b) and Table S3]. Compared to 2PACz, which lacks a passivation group, the reduced PL intensity for ITO/thienyl-substituted carbazole-type SAM/perovskite devices is considered to be due to enhanced hole extraction as a result of the suppression of charge recombination at the interface between the perovskite and SAM. On the other hand, the ITO/thienyl-substituted carbazole-type SAM/perovskite devices exhibits similar PL decay times, although no differences in the PL intensity due to alkyl chain length are observed.

Effective coverage of on ITO surface by hole-collecting molecules is critically important for hole extraction in PSCs.[32] The number of molecules adsorbed onto a conducting surface can be estimated from cyclic voltammograms by observing whether the oxidation peak intensity varies with the scan rate (Fig. S12). Monolayer films of all SAMs were prepared on ITO by spin coating from EtOH solutions. The data are summarized in Table S4. In the case of a 2 mM spin-coating solution, the surface density of thienyl-substituted carbazole-type molecules is $\sim 4 \times 10^{13}$ molecules cm^{-2}, which is smaller than that for **2PACz**. In addition, because **T-4PACz** exhibits greater solubility in organic solvents than the other SAMs, 4 mM and 6 mM solutions could be used; thus, the surface density was investigated in these cases as well and was found to increase with increasing solution concentration. However, an excessively high surface density of adsorbed molecules led to a decrease in PCE, as described below. **T-PACz**, **T-2PACz**, and **T-3PACz** exhibit low solubility, precluding the formation of SAMs using a high-concentration solution.

The PSC with **T-4PACz** as the HTL exhibited the highest PCE among all of the devices described above; therefore, to optimize cell performance, we investigated the effect of the **T-4PACz** concentration on various photovoltaic parameters (Table S5 and Fig. 2d and Fig. S13). The PSC prepared using a 1 mM solution exhibits large data variability and a low PCE, whereas the PSC fabricated using a 4 mM solution has the highest PCE. In the PSCs containing HTLs prepared from high-concentration solutions, the SAM cover the ITO surface more effectively, thereby suppressing charge-carrier recombination and improving efficiency. **T-4PACz** has a long alkyl chain, and is therefore highly soluble in organic solvents and can be dissolved to a concentration of ~ 6 mM. By contrast, SAMs with short alkyl chains are poorly soluble and cannot be used to prepare concentrated SAM solutions. Increased adsorption of **T-4PACz** onto the ITO surface reduces charge recombination, thereby improving device performance. However, the results also suggested that a higher density of adsorbed molecules does not necessarily lead to a higher PCE; the use of high-concentration SAM solutions is speculated to impair the film-forming properties and decrease the FF. Fig. 3 shows *J*–*V* curves and EQE spectra for the best-performing PSC based on **T-4PACz** and for the reference PSC based on **2PACz**. The obtained parameters are listed in Table 1. A cross-sectional SEM image of the former PSC is shown in Fig. S14. The projected J_{sc} values for the PSCs based on **T-4PACz** as obtained by integrating the EQE over the 1.5G standard spectrum, is 22.3 and mA cm^{-2},

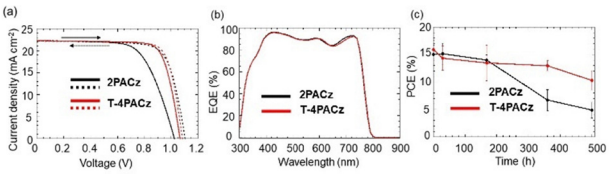

Fig. 3 (a) *J*–*V* curves, (b) EQE spectra and (c) change in efficiency at 65 °C for PSCs based on **2PACz** and **T-4PACz**.

Table 1 Photovoltaic parameters for best-performing PSCs based on **T-4PACz** and **2PACz**, where an antireflection film (MOSMITE) was used on the glass side

SAM	Direction	J_{sc} (mA cm^{-2})	V_{oc} (V)	FF	PCE (%)
2PACz	Forward	22.6	1.07	0.73	17.6
	Backward	22.5	1.10	0.73	18.1
T-4PACz	Forward	22.3	1.07	0.77	18.3
	Backward	22.2	1.08	0.78	18.8

consistent with the value obtained using a solar simulator. In this case, the PSCs were fabricated using an antireflection film (MOSMITE, Mitsubishi Chemical) on the glass side of the devices. The best PCE for the device fabricated with **T-4PACz** is 18.8%, which is higher than that for the PSC based on **2PACz**. Although the J_{sc} and V_{oc} values for the PSC based on **T-4PACz** are approximately the same as those for the PSC based on **2PACz**, the former PSC exhibits a higher FF because of the superior film-forming properties of **T-4PACz**.

The poor long-term stability of PSCs is widely recognized as one of the most important problems that must be overcome for their future commercialization.[33–35] Therefore, we carried out thermal stability tests on PSCs based on **2PACz** or **T-4PACz** encapsulated at 65 °C. As seen in Fig. 3(c), the PCE for the PSC based on **2PACz** decreases to ~30% of its maximum value within 500 h, whereas that for the **PCE** based on **T-4PACz** maintains ~70% of its maximum value. The enhanced thermal stability of PSCs based on **T-4PACz** is attributed to the robustness conferred by passivation of the perovskite surface *via* thienyl groups, and to the suppression of defect-induced degradation pathways.

In summary, we synthesized carbazole-type SAMs (**T-PACz**, **T-2PACz**, **T-3PACz**, and **T-4PACz**) that feature thienyl-substituted carbazole units that are known for their ability to passivate interface defects in perovskite absorber layers. The molecules used to produce the SAMs had alkyl spacers with different lengths. We fabricated PSCs using these SAMs as a HTL and compared the effect of their alkyl spacer length on the device performance. Although the SAMs were found to exhibit similar photochemical properties, differences were observed in the performance of PSC devices fabricated using them. The PSC based on **T-4PACz**, which has butylene spacers, exhibited the highest PCE among the devices investigated. This high PCE is attributed to **T-4PACz** having the highest solubility in organic solvents and excellent film-forming properties. The PSCs fabricated using high-concentration solutions of **T-4PACz** enabled the SAM to cover the ITO surface more effectively, thereby suppressing charge-carrier recombination, enhancing hole extraction, and improving the efficiency and thermal stability compared with the PSCs based on **2PACz**. This work demonstrates the effects of the length of the alkyl spacer on the performance of i-PSCs. In addition, the results obtained here are expected to be useful for optimizing SAM properties and studying novel molecular designs in the future.

Conflicts of interest

There are no conflicts to declare.

Data availability

The data supporting this article have been included as part of the supplementary information (SI). The supplementary information contains detailed experimental procedures, NMR data, and supporting figures and tables. See DOI: https://doi.org/10.1039/d6cc01405d.

Acknowledgements

This research was financially supported by New Energy and Industrial Technology Development Organization (NEDO, JPNP21016).

References

1 A. Kojima, K. Teshima, Y. Shirai and T. Miyasaka, *J. Am. Chem. Soc.*, 2009, **131**, 6050–6051.
2 J. T. Michael, M. Lee, T. Miyasaka, T. N. Murakami and H. J. Snaith, *Science*, 2012, **338**, 643–647.
3 M.-I. Jamesh, H. Tong, M. Du, W. Niu, G. Jia, K.-C. Cheng, C.-W. Hsieh, H.-H. Shen, B. Xu, Y. Tian, X. Xu and H.-Y. Hsu, *npj Mater. Sustainability*, 2025, **3**, 1, DOI: 10.1038/s44296-025-00073-9.
4 D. He, D. Ma, J. Zhang, Y. Yang, J. Ding, C. Liu, X. Liu, Y. Yu, T. Liu, C. Chen, M. Li and J. Chen, *Adv. Mater.*, 2025, **37**, e2505115.
5 B. Koo, W. Kim, K. Choi, J. Huh and M. J. Ko, *Adv. Mater.*, 2025, **37**, e2505115.
6 L. Zhang, M. Fu, X. Jiang, Z. Zhang, C. Wang, Z. Su, B. He, L. Tang, G. Zheng, X. Gao and J. He, *Adv. Sci.*, 2025, **12**, e12117.
7 Q. Zhou, G. Huang, J. Wang, T. Miao, R. Chen, X. Lei, E. Xu, S. Liu, H. Zhu, Z. Tan, C. Shi, X. Liu, Q. Wang, J. Li, Y. Chen, Q. Chen, Y. Shen, M. Sui, Y. Lu, Z. Liu and W. Chen, *Nat. Energy*, 2025, **10**, 1371–1381.
8 D. Wang, Z. Liu, Y. Qiao, Z. Jiang, P. Zhu, J. Zeng, W. Peng, Q. Lian, G. Qu, Y. Xu, Y. Zhang, F. Li, L. Yan, X. Wang, Y.-G. Wang, A. K. Y. Jen and B. Xu, *Joule*, 2025, 9, DOI: 10.1016/j.joule.2024.101815.
9 T. Wang, X. Pu, J. Yang, J. Li, J. Liu, N. Zhao and Q. Zhang, *Sol. RRL*, 2025, 9, DOI: 10.1002/solr.202500566.
10 X. Luo, X. Liu, X. Lin, T. Wu, Y. Wang, Q. Han, Y. Wu, H. Segawa and L. Han, *ACS Energy Lett.*, 2024, **9**, 1487–1506.
11 R. He, X. Liu, T. Liu, T. Zhao, Y. Chen and Q. Song, *Adv. Funct. Mater.*, 2025, **35**, 2506386.
12 H. Liang, W. Zhu, Z. Lin, B. Du, H. Gu, T. Chen, F. Du, L. Bu, Y. Zhou, X. Xie, Y. Zhu, Y. Lin, W. Yang, N. Zhang, L. Ding, S. Yang and C. Liang, *Angew. Chem., Int. Ed.*, 2025, **64**, e202501267.
13 Y. Huang, T. Liu, D. Li, Q. Lian, Y. Wang, G. Wang, G. Mi, Y. Zhou, A. Amini, B. Xu, Z. Tang, C. Cheng and G. Xing, *Small*, 2022, **18**, e2201694.
14 S. Yu, Z. Xiong, H. Zhou, Q. Zhang, Z. Wang, F. Ma, Z. Qu, Y. Zhao, X. Chu, X. Zhang and J. You, *Science*, 2023, **382**, 1399–1404.
15 A. Magomedov, A. Al-Ashouri, E. Kasparavičius, S. Strazdaite, G. Niaura, M. Jošt, T. Malinauskas, S. Albrecht and V. Getautis, *Adv. Energy Mater.*, 2018, 8, DOI: 10.1002/aenm.201801892.
16 S. Jia, C. Gu, X. Zhou, Y. Miao, Y. Tian, S. Wen, J. Ma and X. Bao, *Adv. Funct. Mater.*, 2025, **36**, e12747.
17 E. K. Amran Al-Ashouri1, B. Li, A. Magomedov, H. Hempel, P. Caprioglio, J. A. Márquez, A. B. M. Vilches, E. Kasparavicius, J. A. Smith, N. Phung, D. Menzel, M. Grischek, L. Kegelmann, D. Skroblin, T. M. C. Gollwitzer, M. Jošt, G. Matic, B. Rech, R. Schlatmann, M. Topic, L. Korte, A. Abate, B. Stannowski, M. S. D. Neher, T. Unold, V. Getautis and S. Albrecht, *Science*, 2020, **370**, 1300–1309.
18 L. Jia, S. Xia, J. Li, Y. Qin, B. Pei, L. Ding, J. Yin, T. Du, Z. Fang, Y. Yin, J. Liu, Y. Yang, F. Zhang, X. Wu, Q. Li, S. Zhao, H. Zhang, Q. Li, Q. Jia, C. Liu, X. Gu, B. Liu, X. Dong, J. Liu, T. Liu, Y. Gao, M. Yang, S. Yin, X. Ru, H. Chen, B. Yang, Z. Zheng, W. Zhou, M. Dou, S. Wang, S. Gao, L. Chen, M. Qu, J. Lu, L. Fang, Y. Wang, H. Deng, J. Yu, X. Zhang, M. Li, X. Lang, C. Xiao, Q. Hu, C. Xue, L. Ning, Y. He, Z. Li, X. Xu and B. He, *Nature*, 2025, **644**, 912–919.
19 S. Casalini, C. A. Bortolotti, F. Leonardi and F. Biscarini, *Chem. Soc. Rev.*, 2017, **46**, 40–71.
20 A. Al-Ashouri, A. Magomedov, M. Roß, M. Jošt, M. Talaikis, G. Chistiakova, T. Bertram, J. A. Márquez, E. Köhnen, E. Kasparavičius, S. Levcenco, L. Gil-Escrig, C. J. Hages, R. Schlatmann, B. Rech, T. Malinauskas, T. Unold, C. A. Kaufmann, L. Korte, G. Niaura, V. Getautis and S. Albrecht, *Energy Environ. Sci.*, 2019, **12**, 3356–3369.
21 W. Jiang, M. Liu, Y. Li, F. R. Lin and A. K. Jen, *Chem. Sci.*, 2024, **15**, 2778–2785.
22 J. M. Ramon, J. G. Sanchez, M. Mas-Montoya, W. Li, E. Martinez-Ferrero, E. Palomares and D. Curiel, *Small*, 2025, **21**, e2500067.
23 T. Y. Wen, S. Yang, P. F. Liu, L. J. Tang, H. W. Qiao, X. Chen, X. H. Yang, Y. Hou and H. G. Yang, *Adv. Energy Mater.*, 2018, 8, DOI: 10.1002/aenm.201703143.

24 F. Toniolo, L. Pancini, A. Oranskaia, N. Mrkyvkova, P. Siffalovic, R. Pallotta, M. Degani, F. Doria, U. Schwingenschlögl and G. Grancini, *Sol. RRL*, 2025, 9, DOI: 10.1002/solr.202500582.
25 J. Wan, Z. Zhang, J. Lin, Z. Li, H. Liu, Q. Li, S. Yang and L. Wang, *J. Mater. Chem. C*, 2024, **12**, 15644–15653.
26 X. Ai, Q. Cheng, Z. Lu, C. Gao, Y. Liu, Q. Cao, J. Wu, L. Li, Y. Han, L. Han, G. Yu, G. Zhang, H. Hu, J. Li, Y. Wang and H. Lin, *J. Mater. Chem. A*, 2025, **13**, 33846–33854.
27 C. Li, Z. Zhang, H. Zhang, W. Yan, Y. Li, L. Liang, W. Yu, X. Yu, Y. Wang, Y. Yang, M. K. Nazeeruddin and P. Gao, *Angew. Chem., Int. Ed.*, 2024, **63**, e202315281.
28 C. Edmiston and K. Ruedenberg, *Rev. Mod. Phys.*, 1963, **35**, 457–464.
29 J. Burschka, F. Kessler, M. K. Nazeeruddin and M. Grätzel, *Chem. Mater.*, 2013, **25**, 2986–2990.
30 A. Kogo, R. Ishikawa and T. N. Murakami, *ACS Appl. Energy Mater.*, 2024, **7**, 7769–7774.
31 A. Kogo and T. N. Murakami, *ChemPhysChem*, 2023, **24**, e202200832.
32 M. A. Truong, T. Funasaki, L. Ueberricke, W. Nojo, R. Murdey, T. Yamada, S. Hu, A. Akatsuka, N. Sekiguchi, S. Hira, L. Xie, T. Nakamura, N. Shioya, D. Kan, Y. Tsuji, S. Iikubo, H. Yoshida, Y. Shimakawa, T. Hasegawa, Y. Kanemitsu, T. Suzuki and A. Wakamiya, *J. Am. Chem. Soc.*, 2023, **145**, 7528–7539.
33 G. Feng, T. Wang, X. He, H. Chen, W. Lu, Z. Zhou, Q. Cao and X. Li, *Nano Energy*, 2025, **141**, 111084.
34 Q. Jiang, J. Tong, Y. Xian, R. A. Kerner, S. P. Dunfield, C. Xiao, R. A. Scheidt, D. Kuciauskas, X. Wang, M. P. Hautzinger, R. Tirawat, M. C. Beard, D. P. Fenning, J. J. Berry, B. W. Larson, Y. Yan and K. Zhu, *Nature*, 2022, **611**, 278–283.
35 L. Xu, W. Qian, Y. Zhou, Z. Wei, H. Wang, W. Lv, J. Li, W. Huang, L. Yao, R. Chen and W. Huang, *Angew. Chem., Int. Ed.*, 2025, **64**, e202503702.